Applied Surface Science 505 (2020) 144449

Contents lists available at ScienceDirect

Applied Surface Science

journal homepage: www.elsevier.com/locate/apsusc

Full Length Article

Green synthesis of silver nanostructures with amino acid-modified Pluronic F127 for antibacterial applications

Douglas C. Santos[a,*], João M.R. Goes[b], Viviane C. de Souza[c], Diego Fonseca Bispo[b,c], Larissa Otubo[d], George R.S. Andrade[a,e], Zaine Teixeira Camargo[c,*], Euler A. dos Santos[a]

[a] Department of Materials Science and Engineering, Federal University of Sergipe, São Cristóvão, SE, Brazil
[b] Department of Chemical Engineering, Federal University of Sergipe, São Cristóvão, SE, Brazil
[c] Postgraduate Program in Chemistry, Federal University of Sergipe, São Cristóvão, SE, Brazil
[d] Nuclear and Energy Research Institute (IPEN), National Nuclear Energy Commission (CNEN), São Paulo, Brazil
[e] Postgraduate Program in Energy, Federal University of Espírito Santo, São Mateus, ES, Brazil

ARTICLE INFO

Keywords:
Silver nanoparticles
Pluronic
Amino acids
Photoreduction
Antibacterial activity

ABSTRACT

The aim of this work was to evaluate the use of amino acid-functionalized Pluronic F127 derivatives in the synthesis of silver nanostructures (SNS), such as nanoparticles (SNP) and nanoclusters (SNC). Herein, glycine, L-alanine, and DL-alanine were used to functionalize poly(ethylene oxide) (PEO) end groups from the polymer chain via an esterification pathway. The esterified polymers were used for reducing and stabilizing SNS by a hydrothermal or a photo-assisted route (using a UVA light). The functionalized polymers were characterized by FTIR and the obtained SNS were characterized by UV–vis spectroscopy and TEM, which showed that the SNS obtained by the hydrothermal route are predominantly spherical, whereas those obtained by photo-assisted method give rise to rods and prisms. Kinetic studies showed that alanine and glycine form particles with different rates and that the different enantiomers (L and DL) influence the size and shape of SNS. The nanoparticles obtained by the two routes had their antibacterial efficiency tested against *S. aureus* by the Agar well diffusion method.

1. Introduction

Metal nanostructures are one of the main research subjects in nanotechnology, especially the noble metal nanostructures such as silver nanostructures (SNS), used in catalysis applications [1], biosensors [2], optics [3] and mainly as antibacterial agent [4]. The latter one is the SNS main application widely used in biomedicine, for the treatment of biomaterial surfaces as an example [5]. The properties of the SNS are strongly linked to the size and shape of the nanostructure, which is a consequence of the synthesis process. [6].

The most common method to obtain metallic nanoparticles in solution is the Turkevich method, in which sodium citrate is used in the reduction and stabilization of nanoparticles, originates particles with a mean size of 20 nm [7]. In order to obtain smaller silver nanoparticles (SNP), with diameters from 10 nm to 15 nm, sodium borohydride is also added so that the borohydride acts as a reducing agent while the citrate acts as a stabilizing agent [8]. However, SNPs obtained using borohydride require purification for instance in biological applications, which can cause changes in the SNP systems, such as in their sizes and shapes [9].

Therefore, methods that allow the direct use of the nanoparticles, without the need for subsequent purification steps have been sought. Natural and synthetic biocompatible polymers have been widely explored in this sense [10,11]. In this regard, Pluronic®, an amphiphilic copolymer composed of hydrophilic segments of polyethylene oxide (PEO) and hydrophobic segments of polypropylene oxide (PPO) in "ABA" type (-PEO-PPO -PEO-), has been used efficiently to both to reduce and to stabilize metallic nanoparticles [12,13]. The main advantages of using Pluronic is its high biocompatibility, low bioaccumulation as well as biofilm anti-adhesion property, which greatly

Abbreviations: SNS, silver nanostructures; SNP, silver nanoparticles; SNC, silver nanoclusters; PEO, poly(ethylene oxide); PPO, poly(propylene oxide); FTIR, Fourier-transform infrared spectroscopy; UV–vis, ultraviolet–visible; TEM, transmission electron microscopy; Pluronic F127, P127; L-alanine, L-Ala; D,L-alanine, DL-Ala; glycine, Gly; AA, amino acid; c.m.c., critical micellar concentration; ANOVA, analysis of variance; SD, standard deviation; FWHM, full width at half maximum; SPR, surface plasmon resonance

* Corresponding authors.
E-mail addresses: mscdouglas30@gmail.com (D.C. Santos), zaineteixeira@ufs.br (Z.T. Camargo).

https://doi.org/10.1016/j.apsusc.2019.144449
Received 2 July 2019; Received in revised form 12 October 2019; Accepted 17 October 2019
Available online 31 October 2019
0169-4332/

expands its applications in the area of biomaterials [14].

The SNP obtained using Pluronic® F127 already have been reported in the literature by hydrothermal and by photo-assisted routes, and in both cases the particle size range was 30–40 nm, which makes them uninteresting for some applications, such as bacteria control, where smaller dimensions are desirable for making the nanoparticles more effective in the action against different microorganisms [15,16].

An alternative to obtain smaller silver nanoparticles is the use of species that have available amino group, since there is an interaction between free electrons of the nitrogen, which acts as an electron donor species (polyanion), and the surface of SNP or silver nanoclusters (SNC), which promotes a more effective stabilization of the SNS and in turn limits their growth [17]. The biocompatibility of SNS can be improved using amino acids, since they are usually found in abundance in living beings. For example, amino acids decreased the toxicity of SNP in mammalian cells [18].

The reducing and stabilizing capacity of an amine compound was explored using octadecylamine (ODA) to obtain SNP in ethanol solution at 70 °C. An increase in ODA molar ratio not only decreased the size of the particles but also made their distribution slightly narrower, with sizes varying from 20 nm to 8 nm [19].

Tyrosine and tryptophan, two essential amino acids, was used as reducing and stabilizing agents in the synthesis of SNP in KOH. After dialysis, SNP with mean sizes of 15 and 20 nm were used in the fabrication of SNP/Agar nanocomposite films by casting method. The films were very efficient against *Lysteria monocytogenesis* and *Escherichia coli* [20].

Glycine is the simplest structure amino acid existing and also the most abundant in the human body as well as the only one that does not present chirality [21]. Alanine has a greater structural complexity with a non-reactive methyl group and one of its isomers, L-alanine, is present in the primary structure of several proteins.

The association of additives as an amine with polymers or surfactants generally changes their physicochemical characteristics, such as the degree of ionization, reaction rates as well as phase separation or clouding [22,23]. For example, the hydrogel of Pluronic F127 in which the hydroxyl end groups were chemically modified to methacryloyl-depsipeptide showed tailored degradation rate by altering the structure of the depsipeptide unit, by using several α-hydroxy acids and different amino acids, including L-alanine. In addition, gelation temperature slightly increased [24].

As far as we are aware, few works describe the use of polymers amine-terminated in the one-step synthesis and stabilization of metal nanoparticles. Block copolymers Surfonamine® (PEO-PPO-NH_2) were used in obtaining gold nanoparticles. The affinity of the amino group for the surface of the nanoparticles played an important role in the stabilization of the nanoparticles, according to the mechanisms proposed by the authors, and no other reducing or stabilizing agent was necessary to obtain the nanoparticles [25]. In this work, Pluronic® F127 has been functionalized by esterification with glycine, L-alanine, and D,L-alanine, so that the amino groups are available at their chain ends. These functionalized polymers were used to obtain SNS, both by hydrothermal route and by photosensitization, evaluating the effect of the method, concentration of the polymer and the different functionalizing amino acids on the size of the SNS. The obtained SNS also had their action evaluated against the bacterium *Staphylococcus Aureus* by the Agar well diffusion method.

2. Experimental section

2.1. Reagents

All the chemicals used in this work were of analytical grade and used without further purification: Pluronic F127, (Sigma-Aldrich, HO$(CH_2\text{-}CH_2\text{-}O)_{100}(CH(CH_3)CH_2\text{-}O)_{65}(CH_2CH_2O)_{100}H$, "PF127"), toluene (Synth, $C_6H_5CH_3$), glycine (Sigma-Aldrich, NH_2CH_2COOH, "Gly"), L-alanine (Sigma-Aldrich, $CH_3CH(NH_2)COOH$, "L-Ala"), D,L-alanine (Sigma-Adrich, $CH_3CH(NH_2)COOH$, "DL-Ala"), silver nitrate (Sigma-Aldrich, $AgNO_3$), ethanol (Synth, C_2H_5OH), chloroform (Synth, $CHCl_3$). MILLI-Q ultrapure water (resistivity around 18.2 MΩ cm at 25 °C) was used throughout.

2.2. Preparation of amino acid-functionalized Pluronic F127 derivatives (AA-PF127)

For the functionalization of PF127 with Gly, L-Ala, and DL-Ala it was used a method previously reported by BOURGEAT-LAMI and GUYOT, 1997, [26] and adapted by our research group. Initially, 3.0 g (0.24 mmol) of Pluronic® F127 was solubilized in 50 mL of toluene and distilled at 105 °C for 3 h in order to remove moisture from the commercial polymer. After distillation, 2.4 mmol of the AA (Gly, L-Ala or DL-Ala) was added to the reaction vessel and the mixture was placed in reflux for 24 h at 110 °C. Then, the solvent was removed by rotevaporation, and the obtained product was resolubilized in chloroform (5 mL) and precipitated in ethyl ether at 4 °C (20 mL), forming a white precipitate. The samples were named as following: PF127/Gly, PF127/L-Ala and PF127/DL-Ala for PF127 functionalized with Gly, L-Ala, and D, L-alanine, respectively.

2.3. Preparation of SNS using aminoacid-functionalized Pluronic PF127

2.3.1. Hydrothermal route

In a typical experiment, 0.315 g of AA-PF127 was suspended in 24.7 mL water and then 0.3 mL of a 20 mmol L^{-1} $AgNO_3$ was added to the reaction vessel. The mixture was stirred for 5 min, transferred to an autoclave (Teflon, 50 mL) and kept under magnetic stirring for 24 h at 140 °C in a silicone bath. The same procedure was performed for non-functionalized PF127. The product obtained was stored under refrigeration.

2.3.2. Photo-assisted method

For the photo-assisted route, a method reported by YAHYAEI & AZIZIAN (2013) was adapted [16]. Initially, 0.126 g of AA-PF127 was added in 5 mL of ethanol and stirred for 5 min. Then, 100 µL of an aqueous 20×10^{-3} mol L^{-1} $AgNO_3$ solution was added to the polymer solution and the volume was adjusted with ethanol to 10 mL, so the final concentrations of the polymer and $AgNO_3$ were 1×10^{-3} mol L^{-1} and 0.2×10^{-3} mol L^{-1}, respectively. Finally, 3.5 mL of this mixture was transferred to a quartz cuvette, placed in a photochemical reaction instrument equipped with a black light fluorescent tube (6 W, 330 lm, λ range = 320–400 nm) and irradiated for 15 min. Temporal measurements of the UV–vis absorbance were performed to verify the particle formation kinetics. The same procedure was used for the non-functionalized polymer.

2.4. Antibacterial activity assay

The antimicrobial activity of the as-prepared samples was studied by the Agar well diffusion test. Gram-positive bacteria *Staphylococcus aureus* (ATCC 25923) donated by the National Institute for Quality Control in Health (INCQS-Fiocruz) and chosen because they are nosocomial pathogens commonly responsible for biofilm-related infections. Initially, all apparatus and materials were autoclaved at 120 °C for 15 min and handled under sterile conditions during the experiments.

In a laminar flow, approximately 30 mL of the autoclaved nutrient agar solution was deposited on each plate. After 2 h, the autoclaved test tube was drilled in the nutrient agar, forming a "well" in the center of the plate. Each well received the addition of 200 µL of the agar solution. After 15 min, 100 µL of the sample suspensions (PF127 + SNS, PF127/Gly + SNS, PF127/L-Ala + SNS, PF127/DL-Ala + SNS) were added to the wells. The effect of the polymers PF127, PF127/DL-Ala, PF127/L-Ala, and PF127/Gly, at a concentration of 1 mmol L^{-1} without the

presence of SNS was also evaluated.

After diffusion of the solution from the well to the culture medium, the bacteria were inoculated, and all samples were produced in triplicate. Staphylococcus aureus bacteria were cultured 24 h before in a Brain heart infusion (BHI) broth, followed by the standard protocol for this procedure. From the broth, using the pre-sterilized soabs, the bacterium was inoculated on all surfaces of the culture medium except for the well.

After the inoculation of the bacteria in the culture medium, the plates were placed in a greenhouse for 24 h at a temperature of 37.5 °C. After this time, the zones of inhibition around the well were measured using ImageJ software. The experiments were done in triplicate and statistical analysis was performed by one way ANOVA, followed by Tukey's multiple comparison test.

2.5. Characterization

2.5.1. FTIR spectroscopy

FTIR measurements were performed in order to characterize the commercial polymer and the ones modified with Gly, L-Ala, and DL-Ala. The FTIR spectra were recorded in a Shimadzu IR Prestige 21 Fourier Transform Infrared Spectrophotometer, with scanning in the range between 4000 and 1000 cm^{-1} at a resolution of 4 cm^{-1} and 64 scans per sample.

2.5.2. UV–vis molecular absorption spectroscopy

The samples were analyzed by UV–vis absorption spectroscopy using a Shimadzu UV-1800 model.

2.5.3.

ectra of the liquid samples were recorded using a Jasco FP-8600.

2.5.4. Transmission electron microscopy (TEM)

The samples were also characterized by TEM using a Jeol JEM-1400 Plus instrument operated at an accelerating voltage of 120 kV. Samples were previously diluted in water (1:10, v/v) and then deposited after sonication in water onto copper grids coated with ultrathin carbon and formvar films.

2.5.5. Dynamic light scattering

Dynamic light scattering (DLS) measurements were performed in order to determine the presence of micelles in both aqueous solutions and ethanol solutions. Measurements were performed in a Malvern Zetasizer Nano ZS.

3. Results and discussion

3.1. Functionalization of Pluronic PF127 with amino acids

In order to verify the functionalization of PF127 with different AA, including Gly, L-Ala, and DL-Ala, FTIR measurements were performed (see Fig. 1). The functionalized and non-functionalized polymers present bands at 2880 cm^{-1} related to symmetric and asymmetric stretching of the aliphatic chain; at 1106 cm^{-1} related to the CO groups and at 1342 cm^{-1} attributed to deformation bands in the OH plane [27]. The spectral differences between the non-functionalized polymer and the functionalized polymers are: (a) the presence of a band around 1590–1550 cm^{-1} in functionalized PF127 spectra, which is attributed to the symmetrical angular deformation of groups ($–NH_2$) [27] and (b) the absence of bands between 1760 and 1700 in functionalized PF127 spectra, which are related to the stretching of groups (-C = O) of amino acid carbonyls [27]. These results suggest that Pluronic F127 was suitably functionalized. Fig. S1 (see Supporting Information) shows the chemical structures for the AA-PF127. It is worth mentioning that the reaction is between the carbonyl group of the amino acid and the hydroxyl groups of the polymer chain, which leaves the amino group

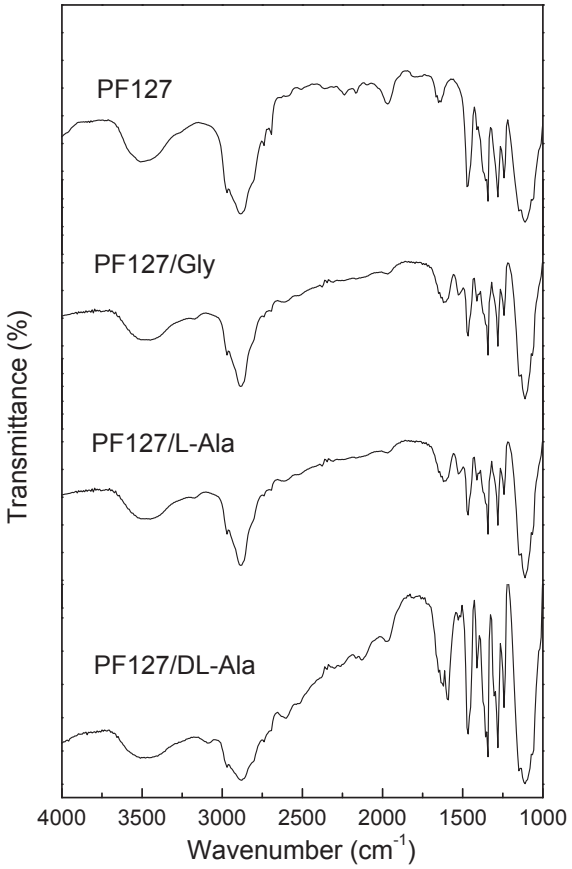

Fig. 1. FTIR spectra of PF127 without functionalization and functionalized with different amino acids.

$–NH_2$ to interact with the nanoparticles.

3.2. Preparation of SNS using aminoacid-functionalized Pluronic PF127

The initial evidence of nanoparticle formation was a change in the color of the solution, which changed from colorless to pale yellow or light brown, as a result of the reduction of Ag^+ ions to Ag^0. The UV–vis spectroscopy was used to study the optical and, consequently, morphological properties such as shape, size, and size distribution of the SNS obtained by different preparation routes. Fig. 2A and B show the UV–vis spectra for the samples prepared by the hydrothermal and the photo-assisted methods, respectively. All the samples were prepared using 1 mmol L^{-1} of the polymer (the non-functionalized PF127 and the functionalized ones with AA). As observed, all spectra present a band at 400–450 nm, which is attributed to the surface plasmon resonance (SPR) band. This band is inherent to colloidal silver nanoparticles and it can vary its intensity, position, and bandwidth when the sample is prepared with different polymers. As known, the SPR band is intrinsically related to the morphological properties of noble metal nanoparticles, such as size (position) and size distribution (bandwidth), as well as concentration (intensity). So, comparing the SPR bands from the as-prepared samples can give some insights about the stabilization promoted by the PF127 and AA-PF127.

As seen in Fig. 2A and Table S1 (see Supporting Information), the sample prepared with DL-Ala presented probably the higher concentration of SNP and the smaller sizes, as its SPR band presented the higher intensity and was centered at the smaller wavelength, respectively. Additionally, DL-Ala presented the smaller bandwidth among all the other samples (which was evaluated by the FWHM values, full width at half maximum). It suggests that this amino acid is able to control the growth of the particles more efficiently, preventing

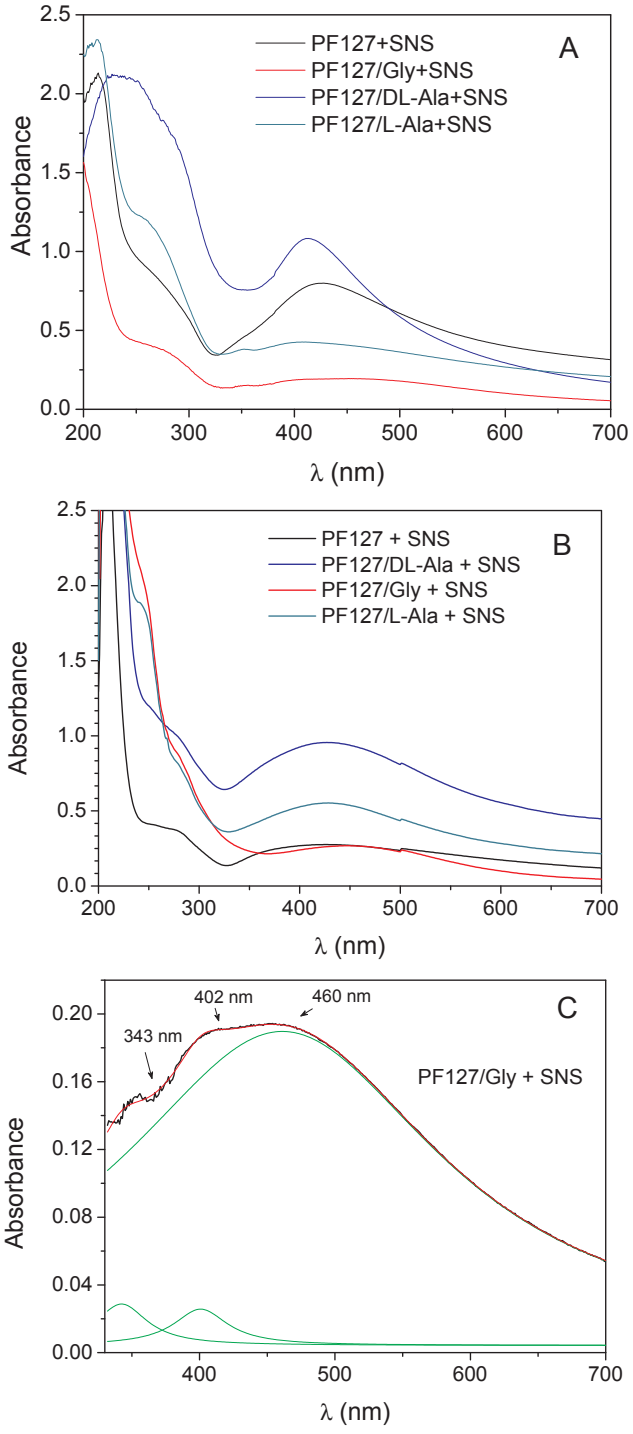

Fig. 2. UV–vis spectra of the SNS obtained by (A) the hydrothermal method, (B) the photo-assisted method and (C) deconvolution of the PF127/Gly spectrum in (A).

aggregation and large size distribution. On the other hand, the spectroscopic data suggest that Gly presented the bigger particles, as its plasmon band is centered at 460 nm. However, it is worth to notice the presence of other contributions at 402 nm and 343 nm, which can be associated with smaller silver nanospheres [28] and with molecular quantum clusters of silver (oligomeric silver species, SNC) [29], respectively. For the samples prepared via the photoreduction method, it is observed that the SPR bands present a redshift (except the one prepared with Gly) and larger FWHM values, suggesting that this method was able to produce larger particles with larger size distribution.

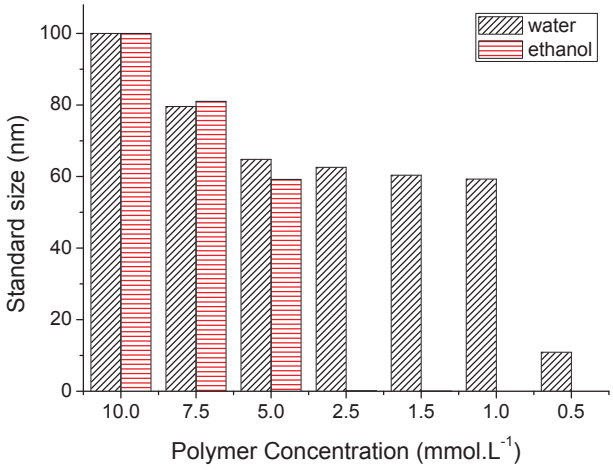

Fig. 3. DLS analysis of PF127 dissolved in water and in ethanol.

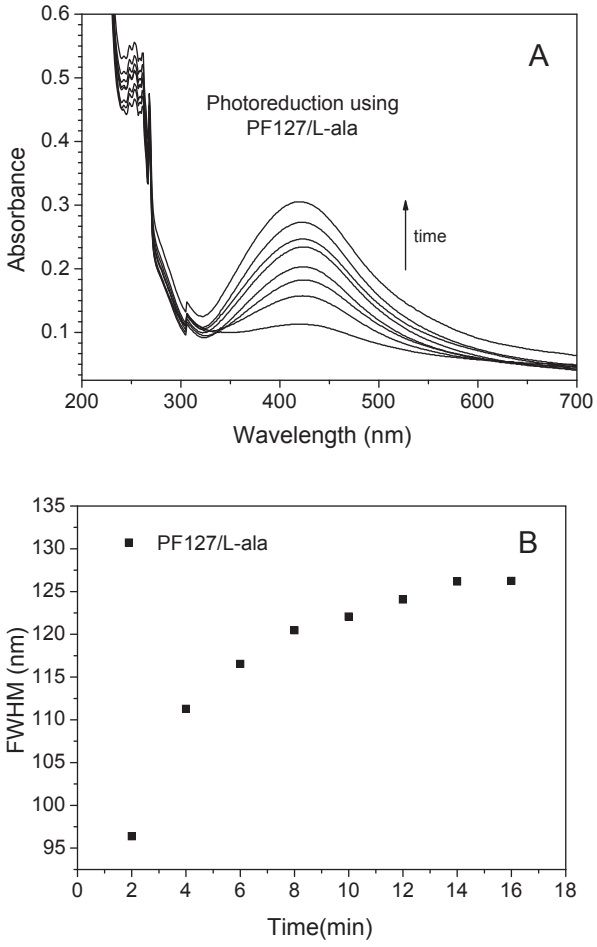

Fig. 4. (A) Kinetic monitoring of the synthesis by photo-assisted route using PF127 + L-Ala, (B) Variation of FWHM as a function of time for the reduced particles in the presence of the PF127/L-Ala.

The effect of PF127 in the formation of nanoparticles in our work is similar to that observed in other studies in the literature, such as the work of SHERVANI et al. (2008), when they obtained silver nanoparticles by action of several polymers, among them Pluronic L64 and P123, without addition of any other reducing agent, obtaining spherical nanoparticles with a dimension between 8 and 24 nm [31]. However, it is known that these SNP have much lower kinetic stability when compared to PF127 [32,33]. In addition, the insertion of the amino group

Table 1
Kinetic parameters obtained from the estimations performed in Statistica software.

Sample	Order	K ± SD	R^2	*p-level*
PF127	1[a]	5.87 ± 0.06 min^{-1}	0.95	0.012
PF127/DL-Ala	2[a]	0.14 ± 0.03 $L\,mol^{-1}\,min^{-1}$	0.95	0.039
PF127/Gly	1[a]	6.41 ± 0.01 min^{-1}	0.93	0.030
PF127/L-Ala	2[a]	1.34 ± 0.03 $L\,mol^{-1}\,min^{-1}$	0.99	0

into the chain of PF127 can be an advantage for the formation and stabilization of nanoparticles, allowing the formation of non-spherical nanoparticles [34].

3.3. Mechanism proposals

3.3.1. Influence of c.m.c

To initiate the discussions regarding the action of the polymer in the formation/stabilization of the nanoparticles by both hydrothermal route and photoassisted route, the presence of polymer aggregation, above its concentration micellar critic (c.m.c.), was firstly investigated in aqueous medium and ethanolic medium by the DLS technique as seen in Fig. 3.

The aqueous or even ethanol solutions above certain concentrations have polymeric agglomerates, frequently termed as micelles [35,36]. Actually, the polymer structure in solution changes from unimers to micelles and finally to micelles with a larger number of monomers or agglomerates of micelles with the increase of the polymer concentration [35,36]. In water, we observed that the micelles become larger, from around 65 nm to 100 nm, as the polymer concentration increases from 5 to 10 mmol L^{-1} (Fig. 3). The size of the micelles has practically no changes from concentrations of 1 to 5 mmol L^{-1} and only a decrease in their number is expected. Possibly there are not more micelles at concentration of 0.5 mmol L^{-1}, since this concentration is below c.m.c. [37]. In the ethanolic solutions, agglomerates are seen from 2.5 to 5 mmol L^{-1} with sizes quite similar to those in water. However, when the concentration is equal or smaller than 2.5 mmol L^{-1}, the number of particles detectable by DLS drops sharply (80%), suggesting that there are no micelles present at this concentration in ethanolic solutions. Thus, in our work there were micelles in the hydrothermal route (in water) but there are not in the photosensitized route (in ethanol).

It is knowing that the amino group has affinity for the SNS surface, binding on them and thus making feasible a more efficient steric stabilization than that promoted by non-functionalized polymer [37]. Thus, we suggest that the insertion of the amino group into the PF127 chain ends directly affects the mechanisms of nanoparticle reduction and stabilization. The interaction between the free electrons of the oxygen present in the polymer chain, in which the main contribution is attributed to the hydrophilic fraction (PEO), is suggested to be responsible for the reduction of the ions of the metal of interest [38]. With the functionalization with amino acids, the free electrons present in the amino group also can contribute to the process of ion reduction [25], as well as, there is an increase of the number of oxygens by the formation of the ester groups between the amino acid and the chain of PF127. The contribution of the unshared electron pair of the nitrogen can increase the number of nuclei, increasing the population of particles and consequently limiting, already in a first stage, the size of the particles by lower availability of ions in solution. Similarly, the amine groups inserted in the polymer chain ends can contribute to the formation of the particles by photosensitization method, since they favor the formation of hydrogen radicals, which are strong reducing agents for metal ions or even act as electron-donor species, activated by UV radiation [39,40].

In addition to the possible contribution to the reduction of ions by the electron donation, the amino groups in the chain ends also has influence on the stabilization of the particles. The adsorption of the PPO groups on the particles may not only be responsible for the limitation of their dimension in the core of micelles but also donate electrons for the reduction of ions [38]. In this way, the positioning of the amino groups at the ends of the chain may favor their adsorption on the surface of the nanoparticles formed instead of the adsorption of the PPO fraction of the polymer. As the chain size is a limiting factor for the shape and size of the particle, possibly the particles adsorbed on the PPO groups are predominantly spherical and present a smaller dimension due to the shape of the micelle nucleus, whereas an unordered adsorption of the amino groups on the particles can favor the growth of these nanoparticles in a uni or bidirectional, which would justify the prismatic

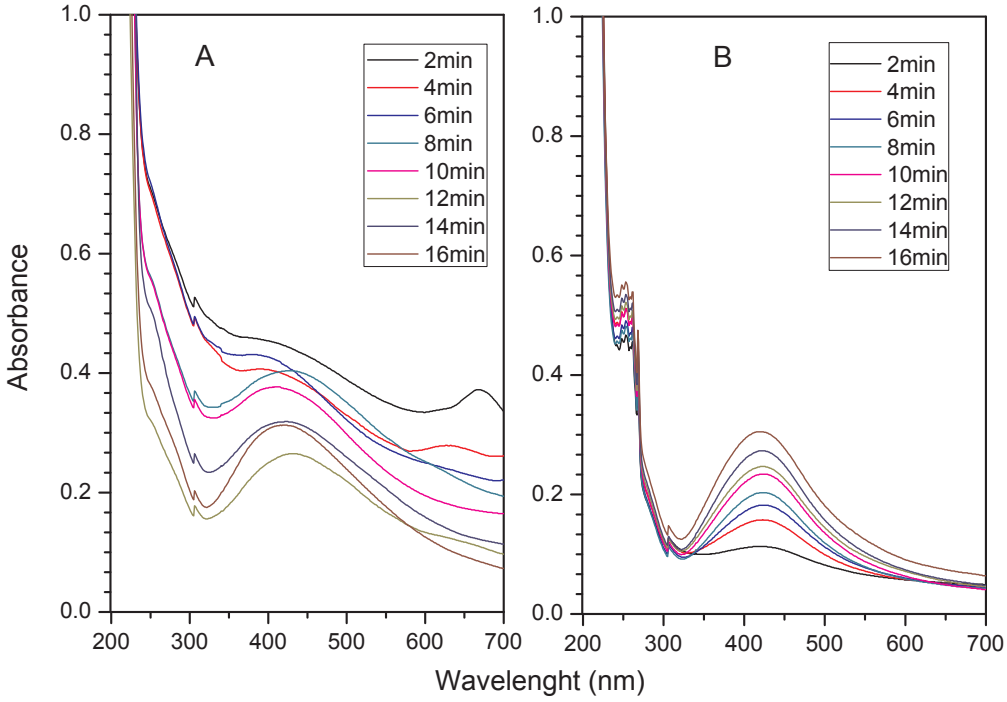

Fig. 5. Spectra of silver nanoparticles obtained in the presence of (A) PF127/DL (B) PF127/L-Ala.

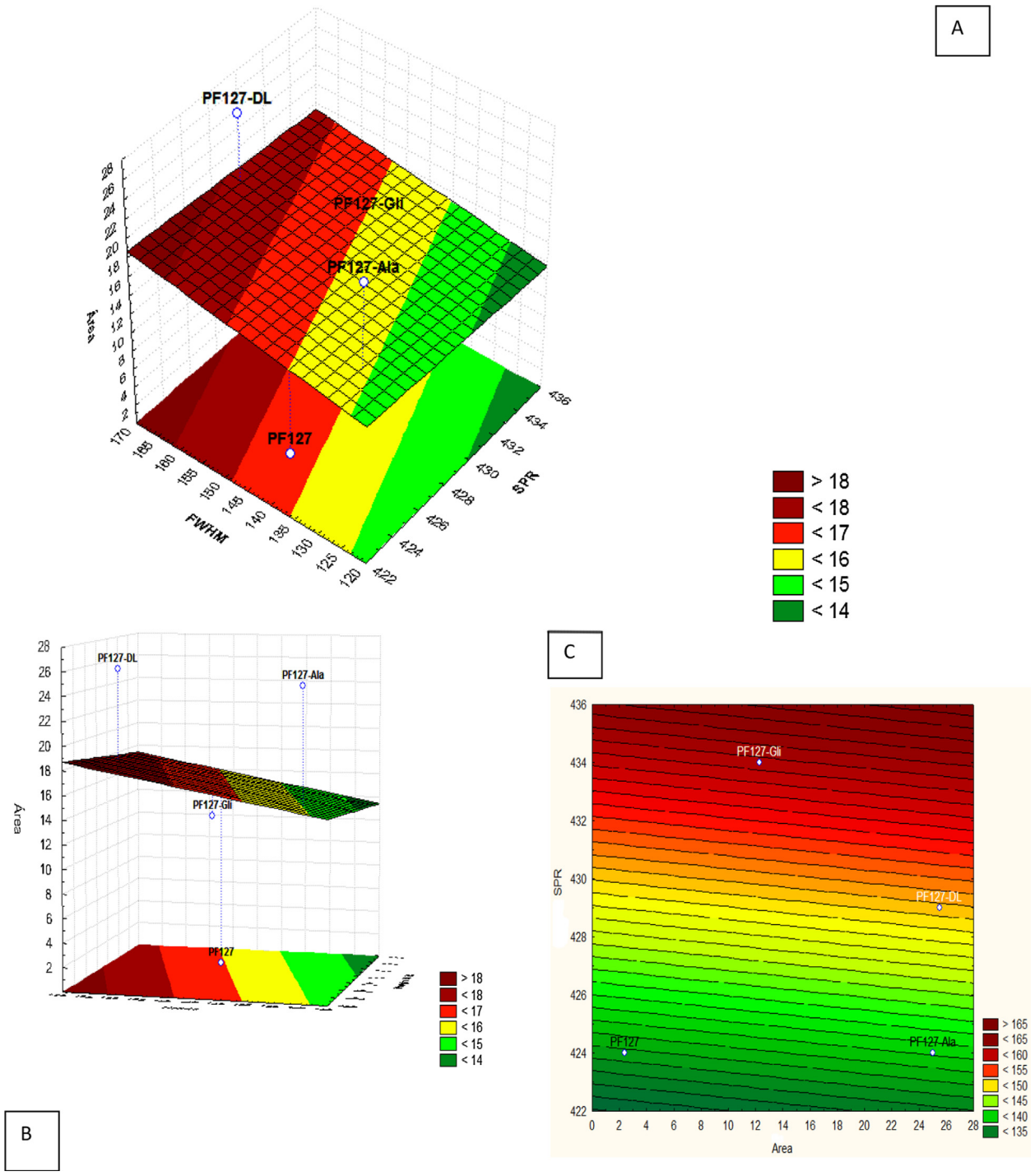

Fig. 6. Response surface constructed based on kinetic data. A - Top view of the response surface B - Side view of the response surface C - Area ratio × SPR obtained by analysis of the response surface.

shape presented by them and a larger size would be justified by the greater availability of crown region space in detriment of nuclei in an aqueous system (see TEM analysis section). Fig. S2 illustrates the proposed organization of particles for the functionalized polymer in the aqueous medium.

On the other hand, the mechanism of the particles obtained by photosensitization is probably mediated by the ethanol with polymers adsorbed on the SNP surface, since there are no micelles in the suspension (Fig. S3). Interestingly, SNC are present only for the systems in which PF127 was functionalized by Gly and D,L-Ala. This is reasonable considering that amine act as capping agent to SNC as well as that more than one amine is probably necessary but cannot stabilize the same cluster due to hysteric hindrance in the L-alanine systems. Actually, this latter is inefficient not only to reduce silver ions in SNC but also in SNP, as discussed based on the Uv–vis and fluorescence spectra as well as the TEM analysis.

Kinetics of SNS formation was evaluated by monitoring the SPR bands, taking as reference the FWHM for the samples prepared by photo-assisted route (Fig. 4).

To evaluate the kinetics of particle formation, the data obtained from each curve were treated according to models described in the literature (15) that define how the kinetics fit a first-order (Eq. (16)), or

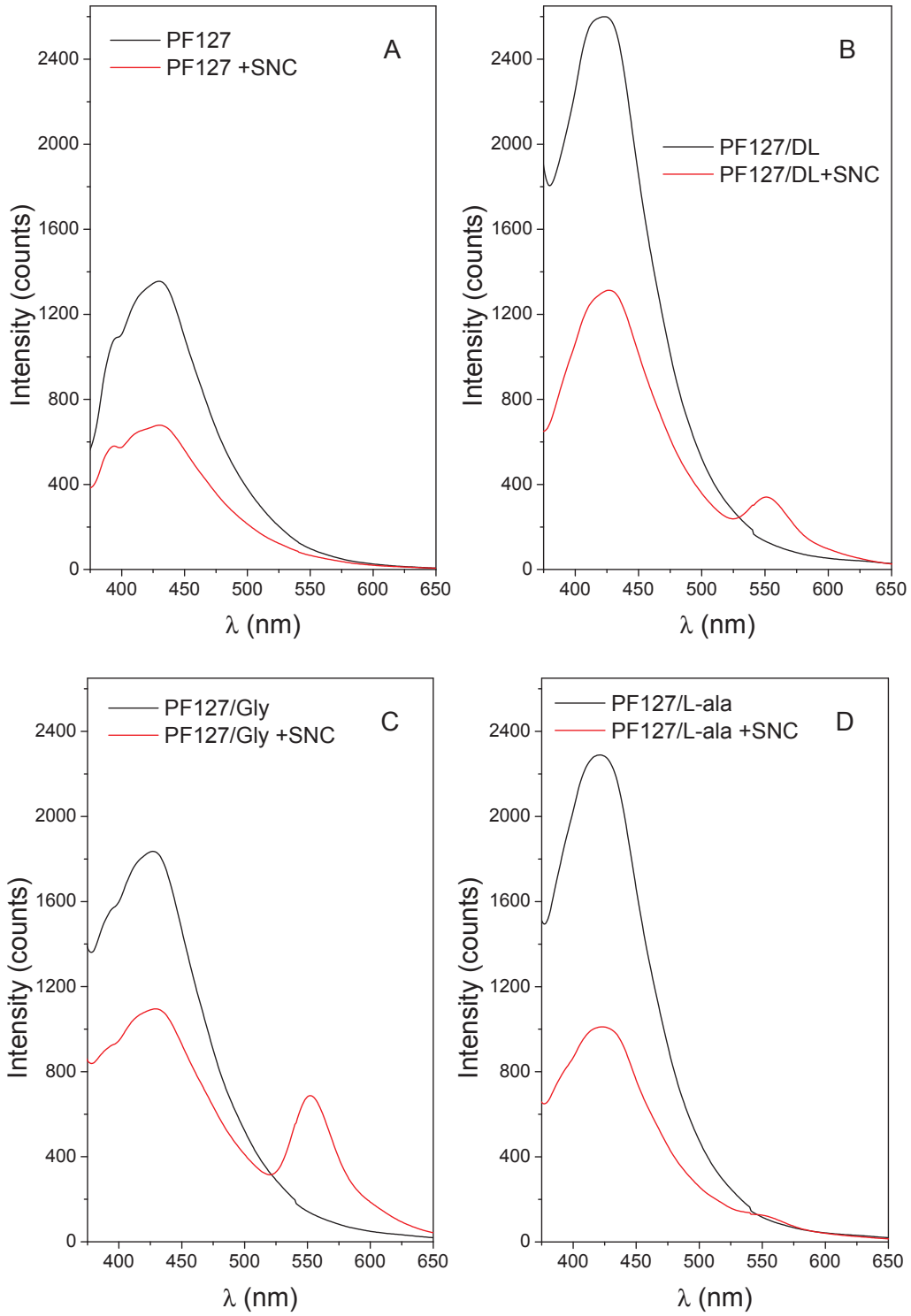

Fig. 7. Fluorescence spectra of the polymers and silver nanoparticles obtained by means of the polymers excited at 350 nm.

second-order model (Eq. (17)), being the adjustment made with the aid of the software STATISTICA, by the method of non-linear regression and by the least-squares method to estimation of the error.

$$A = A_{\infty}(1 - e^{-kt}) \tag{1}$$

$$A = \frac{A_{\infty} kt}{1 + kt} \tag{2}$$

Table 1 was constructed with the results of the estimation of the parameters for each sample along the time of radiation incidence, with the kinetic constant (K), the reaction order, the correlation coefficient of the data (R^2) and the p-level.

Due to variations in the SPR position and width, the kinetic was not monitored by the peak intensity as the only indication of the evolution of the synthesis. The analysis of the FWHM of the spectra considers the effects of particle morphology and dispersion [40].

Based on Table 1 it is possible to observe the differences between the reaction rate of the samples as well as the change in the order of reaction per action of the different functionalizers. Although some samples had a low R^2, the p-level values were below the established

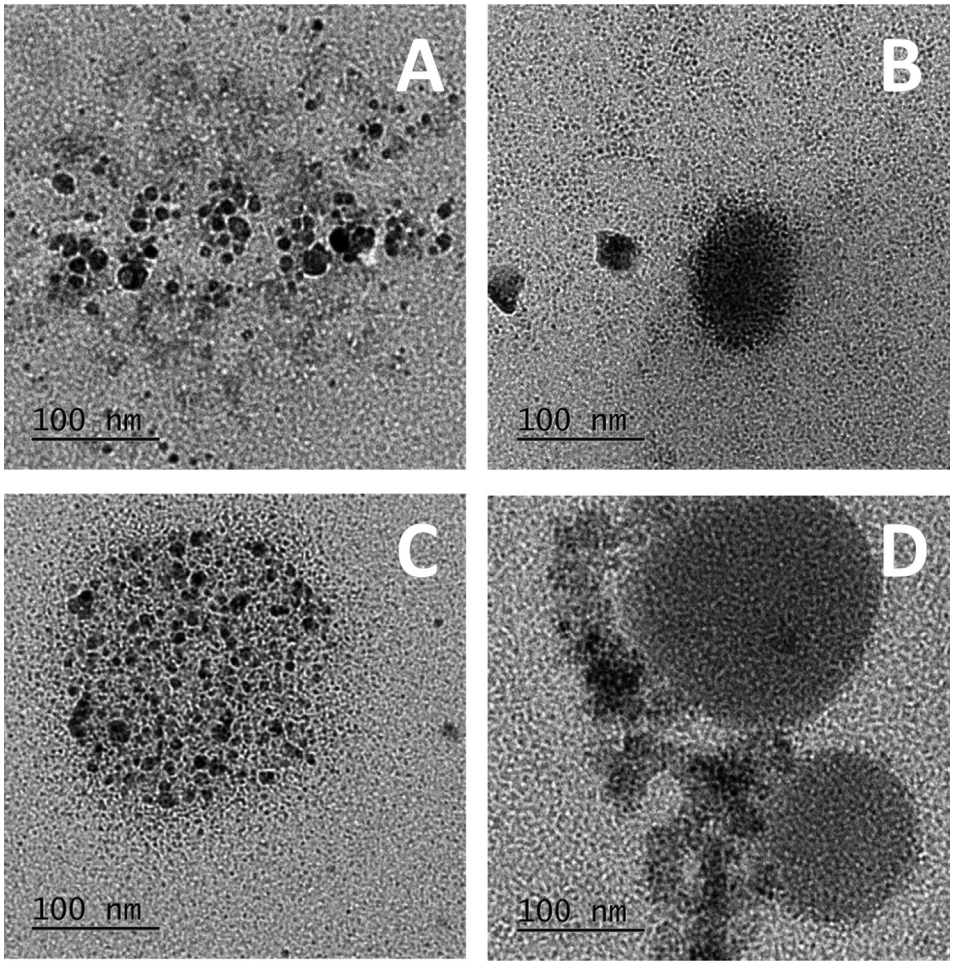

Fig. 8. Transmission electron microscopy image for samples prepared in the presence of (A) PF127 (B) PF127/DL-Ala (C) PF127/Gly (D) PF127/L-Ala.

confidence level ($p < 0.05$), suggesting that the estimates are statistically significant.

Samples obtained using PF127 and PF127/Gly presented a better fit for the first-order equation, with their kinetic constants of 5.80 and 6.42 respectively. The higher rate of particle formation in the presence of PF127/Gly can be attributed to an increase in the availability of electrons by the NH_2 group present in the chain of the esterified polymer, suggesting that the functionalization not only has an effect on the stabilization of the particles but also in the reduction of ions [41].

For the samples in which PF127/DL-Ala and PF127/L-Ala were used, the kinetics became second order with kinetic constants of 0.14 and 1.34 $L\,mol^{-1}\,min^{-1}$ respectively, showing that the increase in the size of the polymer chain and the different enantiomers influence the kinetics of particle formation.

The kinetic and morphological variations of the syntheses are related to the position of the SPR in relation to the size [42], the population of the particles, which can be related to the band area [43], and to the particle size distribution that can be related with FWHM as already mentioned.

In addition to the kinetic evaluation of the SNS, it was also possible to verify if the presence of the different enantiomers would influence the formation of nanoparticles. For this, the evolution curves of the UV–vis spectra were used over time (Fig. 5) for the particles obtained in the presence of the polymer PF127/L-Ala and PF127/DL-Ala.

For the sample in which PF127/DL was used (Fig. 5A), a band above 600 nm was observed in the first 2 min of UV light, for samples in which PF127/L-Ala was used (Fig. 5B) it is not possible to identify the occurrence of such a band, and the baseline is well defined, and it is also evident that during the reaction the SPR increases in intensity, but its position at 421 nm is practically unchanged.

In order to compare the effect of the polymers on the kinetic and population aspects of the solutions, a surface graph was constructed (Fig. 6).

The response surface obtained shows that there is a linear relationship between the variables, as can be seen in Fig. 6A, where the peak area variation in relation to the plasmon band position and FWHM is represented.

The PF127/DL-Ala and PF127/L-Ala samples show a higher particle formation, based on the area values, 25.50 and 25.04 (a.u.) respectively, but they differ in particle size and distribution, since for PF127/L-Ala the distribution is much narrower with FWHM values of 126 nm, which increase to 166.7 nm when the particles are produced in the presence of PF127/DL-Ala. The mean particle size is possibly lower for PF127/L-Ala than PF127/DL-Ala assertion based on the position of the plasmonic bands, located at 424 and 429 nm respectively.

By observing the graph in Fig. 6C, it is verified that the sample in which PF127 was used presents the maximum of its SPR at the shortest wavelength, (SPR = 424 nm), but the smaller the SPR with smaller area equal to 2.41 water, showing that it is a deficient reducing agent compared to the polymers functionalized for the proposed method. However, the PF127/Gly samples have possibly intermediate values in terms of particle population and size distribution, but probably have the largest particles with their SPR located at 434 nm.

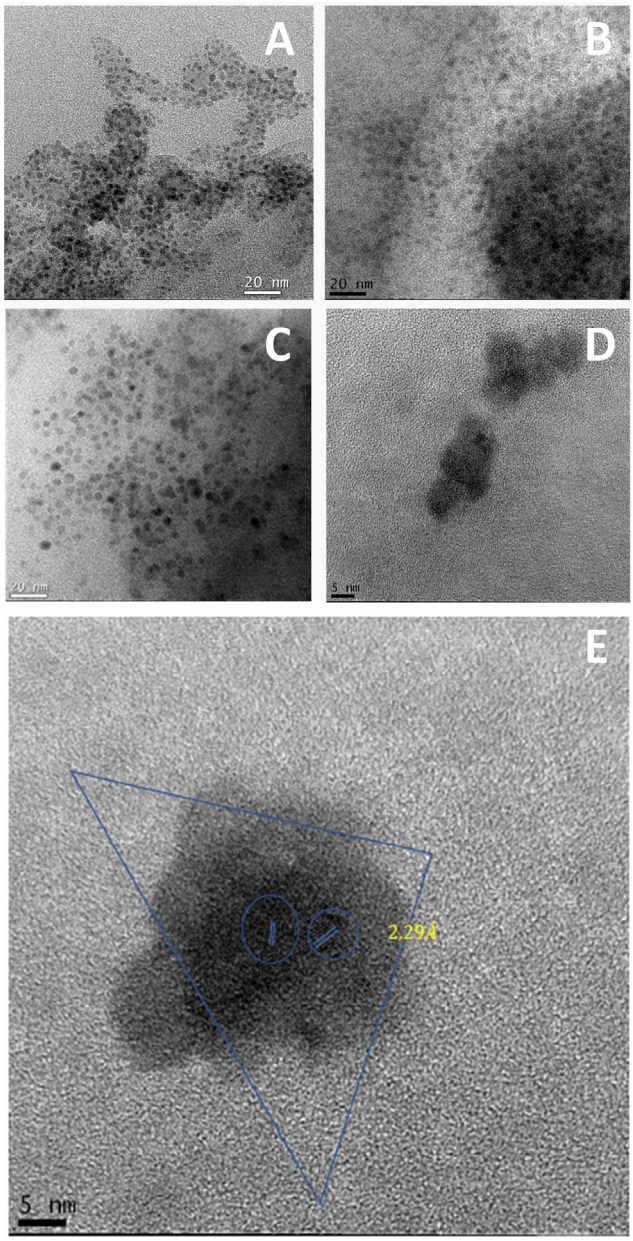

Fig. 9. SNS obtained by (a) 1.5 mmol PF127 (b) 1.5 mmol PF127/DL (c) 1.5 mmol PF127/L-Ala (d) 1.5 mmol PF127/Gly and (e) HRTEM images obtained from sample PF127/Gly + SNS.

3.4. Physical-chemical characterization

The presence of small clusters in some samples was further confirmed by fluorescence measurements. As seen in Fig. 7, the fluorescence spectra of the isolated polymers (functionalized or non-functionalized with amino acids) present an emission band at approximately 430 nm when excited at 350 nm, which is related to the presence of butylated hydroxytoluene (BHT, 2,6-Di-*tert*-butyl-4-methylphenol) [45], an antioxidant additive used by Sigma-Aldrich. After the preparation of the SNS, it is possible to observe some spectral changes. First, a quenching of the emission is observed, which can be a result of an energy transfer from BHT to the noble metal particles. This behavior is expected as the emission band of the donor BHT overlaps the plasmon band and noble metal nanoparticles can act as electrons traps [46].

Additionally, an emission band at 550 nm can also be found in these spectra (except for the non-functionalized PF127), indicating that the as-synthesized Ag clusters were green-emitting. The emission properties of SNCs are frequently related to the number of Ag atoms present in the cluster's core. For instance, Yuan et al. [47] reported the synthesis of red and green emitting SNCs and, according to their data, the samples presented a size-dependent luminescence property, which was corroborated by MALDI-TOF MS analysis. Thus, for the green-emitting SNC, which presented an emission band centered at 500 nm, these authors suggested the presence of a core structure with 9 Ag atoms (Ag9). Among all the samples, the one obtained with PF127-Gly presented the highest emission intensity, which can be correlated with a larger population of clusters. This sample presented the lowest SPR intensity (as shown in Fig. 2), which suggests that the presence of the functionalizing agent increases the stabilization efficiency, giving rise to clusters. The higher stabilization efficiency of PF127/Gly compared to the other two polymers may be associated with the steric availability of the NH_2 group in the glycine molecule, which, because of its affinity for the silver surface, may be responsible for formation of clusters.

The morphology and size of the samples obtained using the different polymers via the hydrothermal method were analyzed by TEM measurements. Representative bright-field TEM image of these samples, available in Fig. 8, shows the presence of SNS in higher contrast with a quasi-spherical morphology. Estimation of average diameters made using ImageJ software showed sizes around 30.0 ± 19.52 nm, 13.77 ± 17.36 nm, 10.50 ± 12.53 nm, and 5.0 ± 3.63 nm for samples prepared with PF127, PF127/L-Ala, PF127/Gly, and PF127/DL-Ala, respectively. These results suggest that the non-functionalized polymer presents a larger size distribution and, consequently, the inability to control the growth/stabilization of the particles when compared with the other amino acid-functionalized pluronic polymers. In general, these results are in accordance with those found in the UV–Vis spectra. For instance, sample PF127/DL + SNS presented the smallest particles and the narrowest size distribution, which reflected to its SPR band (narrower bandwidth and SPR band centered in smaller wavelength), see Table S1 (Supporting Information).

In order to evaluate the morphological properties of these systems varying the stabilizing amount, the samples were prepared with 1.5 mmol L^{-1} of each polymer. As observed in Fig. 9, all the samples also presented SNS in higher contrast with a quasi-spherical morphology. However, the particles were clearly more uniform, smaller and highly dispersed into the polymeric matrixes, which could enhance the antibacterial activity (see the next section). The sample prepared in the presence of PF127/Gly was also analyzed in higher magnification, using a HRTEM instrument. Fig. 9E shows the presence of crystallographic fringes on the surface of the nanoparticles, which presented the distance between the fringes of 2.29 Å. This value is equivalent to the interplanar distance of planes (1 1 1) of silver when the atoms are in a cubic unit centered cubic body (CCC). The presence of this plane can favor the antimicrobial activity, as the surface presents a high electron density [48].

3.5. Antibacterial activity test

The antibacterial activity of the nanoparticles was evaluated by the comparison of the zone of inhibition formed around the well where the samples were deposited. Tests performed with the polymer in the absence of the SNS showed no zone of inhibition, an indication that neither PF127 nor AA-PF127 have antibacterial activity. Besides, all the samples obtained by the hydrothermal route and PF127/L-Ala + SNS, prepared by a photo-assisted route, did not show zone of inhibition. In the experiments using samples obtained by photo-assisted route using PF127/DL-Ala and PF127/Gly, zones of inhibition were seen (Fig. 10).

Table 2 presents the data of the measurements that allow comparing the antibacterial agents in terms of their efficiency. It is possible to notice that gentamicin, a hospital antibiotic that was used as control, presented antibacterial activity with an inhibition zone of around 57 mm. Further, all SNS samples presented smaller inhibition zone in comparison to gentamicin, a hospital antibiotic with molecular

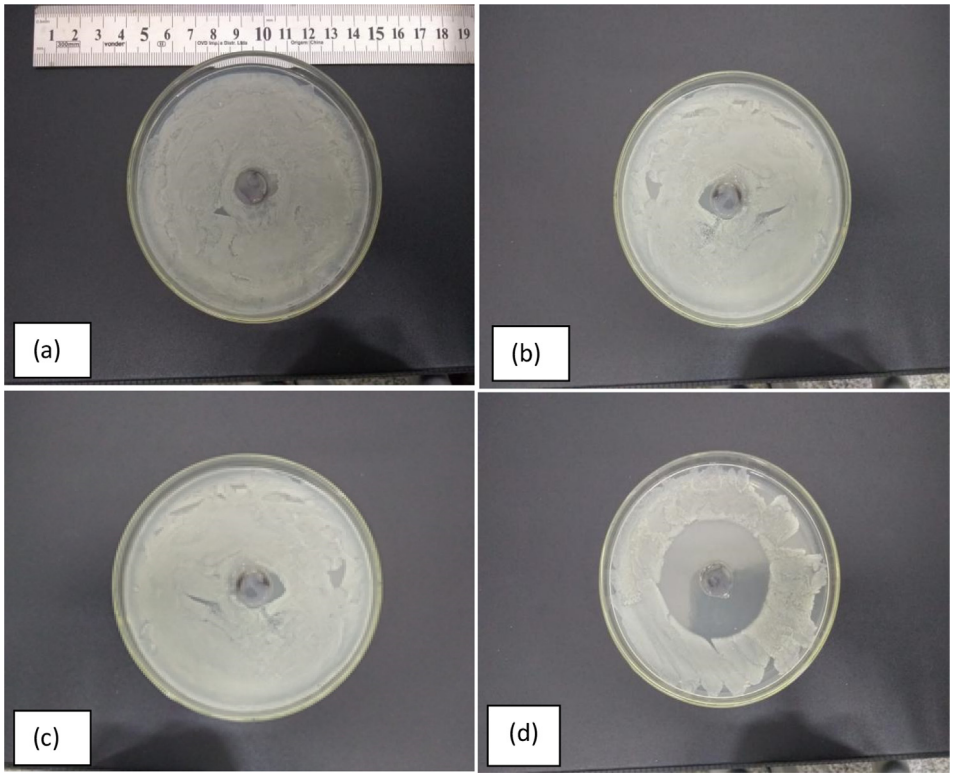

Fig. 10. Images of Petri dishes inoculated with Staphylococcus aureus with inhibition zones formed: (a) PF127/Gly(1.5 mmol L^{-1}) + SNS, (b) PF127/Gly (2 mmol L^{-1}) + SNS, (c) PF127/ DL-Ala(2 mmol L^{-1}) + SNS, (d) Gentamycin.

Table 2
Measurement data of the inhibition zones.

Sample	Zones of inhibition (mm)			Average ± SD (mm)
	Dish 1	Dish 2	Dish 3	
PF127/ Gly(1,5 mmol L^{-1}) + SNS	19.2	20.2	19.0	19.8 ± 0.6[a]
PF127/Gly(2 mmol L^{-1}) + SNS	21.5	19.9	20.7	20.7 ± 0.8[a,b]
PF127/DL-Ala(1,5 mmol L^{-1}) + SNS	16.8	18.6	18.0	17.8 ± 0.9[a]
PF127/DL-Ala(2 mmol L^{-1}) + SNS	20.9	19.9	21.2	20.7 ± 0.6[a,b]
Gentamicin*	56.8	57.0	57.5	57.0 ± 0.4

* positive control; a: $p < 0.0001$ versus Gentamicin and b: $p < 0.05$ versus PF127/DL-Ala (1.5 mmol L^{-1}) + SNS.

structure ($P < 0.0001$). The use of SNS as an antibacterial agent is advantageous in comparison to commercial antibiotics because nanoparticles are effective against resistant microorganisms and have a long efficacy time [49].

According to the literature, decreasing the size of the SNS increases the interaction with bacteria by increasing the penetration through the membrane. This occurs by diffusion for particles smaller than 5 nm and endocytosis for larger particles [48]. We expected that the sample PF127/DL-Ala + SNS and PF127/Gly + SNS prepared by photo-assisted route presented the larger zones of inhibition, since these samples presented the smaller particle sizes along with clusters, as seen by TEM and fluorescence spectra. With respect to the concentration of the polymer, small or no significant changes is expected, since increasing the concentration slightly increases the intensity of the spectra with no changes in the position of bands, which means that probably the efficiency of the reduction is increased and a larger number of particles is present (data not shown). As seen in Table 2, both PF127/Gly (2 mmol L^{-1}) + SNS and PF127/DL-Ala(2 mmol L^{-1}) + SNS produced a significant larger zone of inhibition when compared to PF127/ DL-Ala (1,5 mmol L^{-1}) + SNS ($P < 0.05$), which may be an indication that the antibacterial activity of the samples is strongly correlated to the diffusion of the SNS in the agar medium. Indeed, PF127/Gly was the sample that possesses a higher population of cluster as seen by the fluorescence analysis.

The antibacterial capability of SNC by generating a high concentration of intracellular reactive oxygen species is supposed to be improved in comparison to SNP. Additionally, a lower dosage is needed to possess antimicrobial activity as well as there is a possibility of using their fluorescent properties as a probe for monitoring antimicrobial process. As our samples without SNC did not present antibacterial activity in the concentrations used, we believed that it was because the polymer diminished the diffusion of the SNP from the well. However, SNC would have a higher diffusion because of their smaller sizes.

4. Conclusions

Overall, the insertion of the -NH_2 groups into the Pluronic chain has a distinct influence on the nanoparticles formed via hydrothermal and photo-assisted methods, producing nanoparticles with a narrow size distribution, with predominantly spherical shape. Fluorescence analyses confirmed the presence of metal clusters in the samples obtained by photosensitization using glycine and D,L-alanine. The kinetic studies carried out indicate that the insertion of the amino acid alanine changes the kinetics of the silver nanoparticles to the 2nd order, while the

polymer functionalized with glycine and the nonfunctionalized polymer follows first-order kinetics. The well diffusion tests showed that the nanoparticles obtained through the functionalized polymers show a bacteriostatic action against *Staphylococcus aureus*. The presence of SNC enhanced the bactericidal activity due to its ultra-high surface to volume ratio and unique surface chemistry, being of great interest in the fabrication of antibacterial materials.

Declaration of Competing Interest

The authors declare that they have no conflict of interest.

Acknowledgement

The authors are thankful to the CMNano-UFS (Project no. 63) for the TEM analysis, CNPq (Process no. 476674/2013-1), CAPES, and FAPITEC for financial support. G.R.S.A. received a scholarship from CAPES (PNPD/2016).

Appendix A. Supplementary material

Supplementary data to this article can be found online at https://doi.org/10.1016/j.apsusc.2019.144449.

References

[1] S. Gao, Z. Zhang, K. Liu, B. Dong, Direct evidence of plasmonic enhancement on catalytic reduction of 4-nitrophenol over silver nanoparticles supported on flexible fibrous networks, Appl. Catal. B 188 (2016) 245–252, https://doi.org/10.1016/j.apcatb.2016.01.074.
[2] F. Mazzei, R. Antiochia, P. Bollella, G. Favero, R. Ludwig, C. Schulz, L. Gorton, Green synthesis and characterization of gold and silver nanoparticles and their application for development of a third generation lactose biosensor, Electroanalysis 29 (2016) 77–86, https://doi.org/10.1002/elan.201600476.
[3] S. Pugazhendhi, E. Kirubha, P.K. Palanisamy, R. Gopalakrishnan, Synthesis and characterization of silver nanoparticles from Alpinia calcarata by Green approach and its applications in bactericidal and nonlinear optics, Appl. Surf. Sci. 357 (2015) 1801–1808, https://doi.org/10.1016/j.apsusc.2015.09.237.
[4] Y. Qing, L. Cheng, R. Li, G. Liu, Y. Zhang, X. Tang, J. Wang, H. Liu, Y. Qin, Potential antibacterial mechanism of silver nanoparticles and the optimization of orthopedic implants by advanced modification technologies, Int. J. Nanomed. 13 (2018) 3311–3327, https://doi.org/10.2147/IJN.S165125.
[5] J. Wang, J. Li, G. Guo, Q. Wang, J. Tang, Y. Zhao, H. Qin, T. Wahafu, H. Shen, X. Liu, X. Zhang, Silver-nanoparticles-modified biomaterial surface resistant to staphylococcus: New insight into the antimicrobial action of silver, Sci. Rep. 6 (2016) 1–16, https://doi.org/10.1038/srep32699.
[6] X. Zhang, Z. Liu, W. Shen, S. Gurunathan, Silver Nanoparticles : Synthesis , Characterization , Properties , Applications , and Therapeutic Approaches, (2016). doi:10.3390/ijms17091534.
[7] J. Turkevich, P.C. Stevenson, J. Hillier, A study of the nucleation and growth processes in the synthesis of colloidal gold, Discuss. Faraday Soc. 11 (1951) 55–75, https://doi.org/10.1039/DF9511100055.
[8] S.V. Banne, M.S. Patil, R.M. Kulkarni, S.J. Patil, sciencedirect synthesis and characterization of silver nano particles for EDM applications, Mater. Today: Proc. 4 (2017) 12054–12060, https://doi.org/10.1016/j.matpr.2017.09.130.
[9] A. Burkowska-but, G. Sionkowski, M. Walczak, Influence of stabilizers on the antimicrobial properties of silver nanoparticles introduced into natural water, J. Environ. Sci. 26 (2014) 542–549, https://doi.org/10.1016/S1001-0742(13)60451-9.
[10] R. Jayakumar, D. Menon, K. Manzoor, S.V. Nair, H. Tamura, Biomedical applications of chitin and chitosan based nanomaterials — a short review, Carbohydr. Polym. 82 (2010) 227–232, https://doi.org/10.1016/j.carbpol.2010.04.074.
[11] F. Danhier, E. Ansorena, J.M. Silva, R. Coco, A. Le, V. Préat, PLGA-based nanoparticles : an overview of biomedical applications, J. Control. Rel. 161 (2012) 505–522, https://doi.org/10.1016/j.jconrel.2012.01.043.
[12] A. Pitto-Barry, N.P.E. Barry, Pluronic® block-copolymers in medicine: from chemical and biological versatility to rationalisation and clinical advances, Polym. Chem. 5 (2014) 3291–3297, https://doi.org/10.1039/c4py00039k.
[13] B. Sarkar, V. Venugopal, M. Tsianou, P. Alexandridis, Adsorption of Pluronic block copolymers on silica nanoparticles, Colloids Surf., A 422 (2013) 155–164, https://doi.org/10.1016/j.colsurfa.2013.01.010.
[14] X. Huang, X. Bao, Y. Liu, Z. Wang, Q. Hu, Catechol-functional chitosan/silver nanoparticle composite as a highly effective antibacterial agent with species-specific mechanisms, Scient. Rep. 7 (2017), https://doi.org/10.1038/s41598-017-02008-4.
[15] T. Sakai, A. Ishihara, P. Alexandridis, Block copolymer-mediated synthesis of silver nanoparticles from silver ions in aqueous media, Colloids Surf., A 487 (2015) 84–91, https://doi.org/10.1016/j.colsurfa.2015.09.058.
[16] B. Yahyaei, S. Azizian, Rapid photogeneration of silver nanoparticles in ethanolic solution: a kinetic study, Spectrochim. Acta - Part A: Mole. Biomole. Spectrosc. 101 (2013) 343–348, https://doi.org/10.1016/j.saa.2012.09.093.
[17] J. Natsuki, T. Natsuki, Y. Hashimoto, A review of silver nanoparticles : synthesis methods properties and applications, Int. J. Mater. Sci. Appl. 4 (2015) 325–332, https://doi.org/10.11648/j.ijmsa.20150405.17.
[18] H.K. Daima, P.R. Selvakannan, A.E. Kandjani, R. Shukla, S.K. Bhargava, V. Bansal, Synergistic influence of polyoxometalate surface corona towards enhancing the antibacterial performance of tyrosine-capped Ag nanoparticles, Nanoscale 6 (2014) 758–765, https://doi.org/10.1039/c3nr03806h.
[19] G.M. Neelgund, B. Karthikeyan, S.A. Shivashankar, A. Oki, Single-step, size-controlled synthesis of colloidal silver nanoparticles stabilized by octadecylamine, Appl. Surf. Sci. 356 (2015) 726–731, https://doi.org/10.1016/j.apsusc.2015.07.209.
[20] Amino ShivShankarJong-WhanRhim, acid mediated synthesis of silver nanoparticles and preparation of antimicrobial agar/silver nanoparticles composite films, Carbohydr. Polym. 130 (2015) 353–363.
[21] P. Schemmer, M.D. Wheeler, Glycine reduces platelet aggregation, Amino Acids 44 (2014) 925–931, https://doi.org/10.1007/s00726-012-1422-8.Glycine.
[22] M. Rahman, M.A. Khan, M. Abdul Rub, Md.A. Hoque, A.M. Asiri, Investigation of the effect of various additives on the clouding behavior and thermodynamics of polyoxyethylene (20) sorbitan monooleate in absence and presence of ceftriaxone sodium trihydrate drug, J. Chem. Eng. Data. 62 (2017) 1464–1474, https://doi.org/10.1021/acs.jced.6b01027.
[23] D. Kumar, M.A. Rub, Studies of interaction between ninhydrin and Gly-Leu dipeptide: Influence of cationic surfactants (m-s-m type Gemini), J. Mol. Liq. 269 (2018) 1–7, https://doi.org/10.1016/j.molliq.2018.08.002.
[24] E. Lippens, I. Swennen, J. Gironès, H. Declercq, G. Vertenten, L. Vlaminck, F. Gasthuys, E. Schacht, R. Cornelissen, Cell survival and proliferation after encapsulation in a chemically modified Pluronic(R) F127 hydrogel, J. Biomater. Appl. 27 (2013) 828–839, https://doi.org/10.1177/0885328211427774.
[25] Toshio Sakai, Mai Ishigaki, Tomohiko Okada, Shozi Mishima, A facile route of gold nanoparticle synthesis and surface modification using amino-terminated poly (ethylene oxide)-poly(propylene oxide) block copolymers, J. Nanosci. Nanotech. 10 (2) (2010) 919–926, https://doi.org/10.1166/jnn.2010.1899.
[26] C.P. Sci, S. Verlag, G.C. National, R.S. Laboratoire, C.P.E. Bfit, V. Cedex, Thiol-ended polyethylene oxide as reactive stabilizer for dispersion polymerization of styrene, 729 (1997) 716–729.
[27] R. Silverstein, F. Webster, SPECTROMETRIC IDENTIFICATION OF ORGANIC COMPOUNDS, 6th ed., Wiley India Pvt. Limited, 2006, n.d.
[28] N.G. Bastús, F. Merkoçi, J. Piella, V. Puntes, Synthesis of highly monodisperse citrate-stabilized silver nanoparticles of up to 200 nm: kinetic control and catalytic properties, Chem. Mater. 26 (2014) 2836–2846, https://doi.org/10.1021/cm500316k.
[29] F. Qu, Q. Li, J. You, Fluorescent silver nanoclusters capped by polyethyleneimine with different molecular weights: universal synthesis and application as a temperature sensor, J. Lumin. 177 (2016) 133–138, https://doi.org/10.1016/j.jlumin.2016.04.040.
[31] Z. Shervani, Y. Ikushima, M. Sato, H. Kawanami, Y. Hakuta, T. Yokoyama, T. Nagase, H. Kuneida, K. Aramaki, Morphology and size-controlled synthesis of silver nanoparticles in aqueous surfactant polymer solutions, Colloid Polym. Sci. 286 (2008) 403–410, https://doi.org/10.1007/s00396-007-1784-8.
[32] T. Sakai, P. Alexandridis, Single-step synthesis and stabilization of metal nanoparticles in aqueous pluronic block copolymer solutions at ambient temperature, Langmuir 20 (2004) 8426–8430, https://doi.org/10.1021/la049514s.
[33] Kamil Rahme, Fabienne Gauffre, Jean-Daniel Marty, Bruno Payré, Christophe Mingotaud, A systematic study of the stabilization in water of gold nanoparticles by poly(ethylene oxide) − poly(propylene oxide) − poly(ethylene oxide) triblock copolymers, J. Phys. Chem. C 111 (20) (2007) 7273–7279, https://doi.org/10.1021/jp070274 + .
[34] S. Goy-López, P. Taboada, A. Cambón, J. Juárez, C. Alvarez-Lorenzo, A. Concheiro, V. Mosquera, Modulation of size and shape of au nanoparticles using Amino-X-Shaped poly(ethylene oxide) - Poly(propylene oxide) block copolymers, J. Phys. Chem. B 114 (2010) 66–76, https://doi.org/10.1021/jp908569z.
[35] M.A. Rub, N. Azum, F. Khan, A.M. Asiri, Aggregation of sodium salt of ibuprofen and sodium taurocholate mixture in different media: a tensiometry and fluorometry study, J. Chem. Thermodyn. 121 (2018) 199–210, https://doi.org/10.1016/j.jct.2018.02.019.
[36] D. Kumar, M.A. Rub, Interaction of ninhydrin with chromium-glycylglycine complex in the presence of dimeric gemini surfactants, J. Mol. Liq. 250 (2018) 329–334, https://doi.org/10.1016/j.molliq.2017.11.172.
[37] Y. Deng, J. Li, J. Yu, J. Zhao, J. Tang, Silver nanoparticles well-dispersed in amine-functionalized, one-pot made vesicles as an effective antibacterial agent, Mater. Sci. Eng., C 60 (2016) 92–99, https://doi.org/10.1016/j.msec.2015.11.011.
[38] S.M. Moghimi, A.C. Hunter, Engineering and Experimental Medicine 18 (2000) 2958–2964.
[39] M. Sakamoto, T. Tachikawa, M. Fujitsuka, T. Majima, Two-color two-laser fabrication of gold nanoparticles in a PVA film, Chem. Phys. Lett. 420 (2006) 90–94, https://doi.org/10.1016/j.cplett.2005.12.053.
[40] P.K. Sudeep, P.V. Kamat, Photosensitized growth of silver nanoparticles under visible light irradiation: a mechanistic investigation, Chem. Mater. 17 (2005) 5404–5410, https://doi.org/10.1021/cm0512777.
[41] D.K. Bhui, H. Bar, P. Sarkar, G.P. Sahoo, S.P. De, A. Misra, Synthesis and UV-vis spectroscopic study of silver nanoparticles in aqueous SDS solution, J. Mol. Liq. 145 (2009) 33–37, https://doi.org/10.1016/j.molliq.2008.11.014.
[42] N. Agasti, V.K. Singh, N.K. Kaushik, Synthesis of water soluble glycine capped silver nanoparticles and their surface selective interaction, Mater. Res. Bull. 64 (2015)

17–21, https://doi.org/10.1016/j.materresbull.2014.12.030.
[43] C. Contado, R. Argazzi, V. Amendola, Sedimentation field flow fractionation and optical absorption spectroscopy for a quantitative size characterization of silver nanoparticles, J. Chromatogr. A 1471 (2016) 178–185, https://doi.org/10.1016/j.chroma.2016.10.026.
[45] H.W. Latz, R.J. Hurtubise, Luminescence analysis of food antioxidants; determination of propyl gallate in lard, J. Agric. Food Chem. 17 (1969) 352–355, https://doi.org/10.1021/jf60162a017.
[46] G.R.S. Andrade, C.C. Nascimento, Z.M. Lima, E. Teixeira-Neto, L.P. Costa, I.F. Gimenez, Star-shaped ZnO/Ag hybrid nanostructures for enhanced photocatalysis and antibacterial activity, Appl. Surf. Sci. 399 (2017) 573–582, https://doi.org/10.1016/j.apsusc.2016.11.202.
[47] X. Yuan, M.I. Setyawati, A.S. Tan, C.N. Ong, D.T. Leong, J. Xie, Highly luminescent silver nanoclusters with tunable emissions: cyclic reduction–decomposition synthesis and antimicrobial properties, NPG Asia Mater. 5 (2013) e39, https://doi.org/10.1038/am.2013.3.
[48] G. Hu, W. Jin, Q. Chen, Y. Cai, Q. Zhu, W. Zhang, Antibacterial activity of silver nanoparticles with different morphologies as well as their possible antibacterial mechanism, Appl. Phys. A Mater. Sci. Process. 122 (2016) 1–7, https://doi.org/10.1007/s00339-016-0395-y.
[49] K. Chaloupka, Y. Malam, A.M. Seifalian, Nanosilver as a new generation of nanoproduct in biomedical applications, Trends Biotechnol. 28 (2010) 580–588, https://doi.org/10.1016/j.tibtech.2010.07.006.